

Impact of cosmology dependence of baryonic feedback in weak lensing

Pranjal R. S.,^a Elisabeth Krause,^{a,b} Klaus Dolag,^{c,d} Karim Benabed,^e Tim Eifler,^{a,b} Emma Ayçoberry,^e and Yohan Dubois^e

^aDepartment of Astronomy/Steward Observatory, University of Arizona, 933 North Cherry Avenue, Tucson, AZ 85721, USA

^bDepartment of Physics, University of Arizona, 1118 E Fourth Street, Tucson, AZ 85721, USA

^cUniversitäts-Sternwarte, Fakultät für Physik, Ludwig-Maximilians-Universität München, Scheinerstr. 1, D-81679 München, Germany

^dMax Planck Institute for Astrophysics, Karl-Schwarzschild-Str. 1, D-85741 Garching, Germany

^eInstitut d'Astrophysique de Paris, UMR 7095, CNRS & Sorbonne Université, 98 bis boulevard Arago, F-75014 Paris, France

E-mail: pranjals@arizona.edu

Abstract. Robust modeling of non-linear scales is critical for accurate cosmological inference in Stage IV surveys. For weak lensing analyses in particular, a key challenge arises from the incomplete understanding of how non-gravitational processes, such as supernovae and active galactic nuclei — collectively known as *baryonic feedback* — affect the matter distribution. Several existing methods for modeling baryonic feedback treat it independently from the underlying cosmology, an assumption which has been found to be inaccurate by hydrodynamical simulations. In this work, we examine the impact of this coupling between baryonic feedback and cosmology on parameter inference at LSST Y1 precision. We build mock 3×2 pt data vectors using the *Magneticum* suite of hydrodynamical simulations, which span a wide range of cosmologies while keeping subgrid parameters fixed. We perform simulated likelihood analyses for two baryon mitigation techniques: (i) the Principal Component Analysis (PCA) method which identifies eigenmodes for capturing the effect baryonic feedback on the data vector and (ii) HMCODE2020 [1] which analytically models the modification in the matter distribution using a halo model approach. Our results show that the PCA method is robust to the coupling between cosmology and baryonic feedback, whereas, when using HMCODE2020 there can be up to 0.5σ bias in $\Omega_m - S_8$. For HMCODE2020, the bias also correlates with the input cosmology while for PCA we find no such correlation.

Contents

1	Introduction	1
2	Simulations	3
2.1	Magneticum	3
2.2	Simulations for PCA training	4
3	Impact of cosmology on baryonic feedback	4
4	Simulated likelihood analysis	7
4.1	Theory data vector	7
4.2	Systematics	8
4.3	Baryon mitigation techniques	9
4.4	Mock data	10
4.5	Survey Design	10
4.6	Likelihood and covariance	12
4.6.1	Prior on baryonic feedback parameters	12
5	Results	12
5.1	Performance at the baseline <i>WMAP7</i> cosmology	12
5.2	Baryon mitigation across cosmologies	14
6	Conclusions	16

1 Introduction

The concordance Λ CDM model has been rigorously tested by the current generation of wide-field surveys and has been remarkably successful in explaining a wide range of observations [e.g. 2–10]. However, challenges to the model have also emerged and among the longstanding issues is the discrepancy between the amplitude of matter fluctuations measured at lower redshifts and those predicted by cosmic microwave background (CMB) experiments [e.g. 11]. Upcoming Stage IV weak lensing surveys, such as the Rubin Observatory’s Legacy Survey of Space and Time (LSST¹, [12]), *Nancy Grace Roman Space Telescope* (*Roman*², [13]), and *Euclid*³ [14], will play a crucial role in addressing these issues and exploring extensions to the Λ CDM paradigm.

While non-linear scales probed by weak lensing offer a rich source of information, these scales are subject to a complex interplay between gravitational evolution and baryonic physics. The formation of stars and supermassive black holes in galaxies triggers events such as supernovae and active galactic nuclei (AGN), which inject energy into the surrounding medium. These processes regulate star formation by preventing the collapse of cold gas and expelling it into the circumgalactic and intracluster medium. The redistribution

¹<https://www.lsst.org>

²<https://roman.gsfc.nasa.gov>

³<https://sci.esa.int/web/euclid>

of gas, in turn, induces a gravitational back-reaction on the dark matter halo, further altering the matter distribution. State-of-the-art hydrodynamical simulations have demonstrated that feedback mechanisms can suppress the matter power spectrum by $\mathcal{O}(10\%)$ at $1 \text{ Mpc}^{-1}h < k < 10 \text{ Mpc}^{-1}h$.

Several methods have been developed to address the effects of baryonic feedback in weak lensing analyses. One common strategy is to exclude the range of scales that are not modeled with sufficient accuracy and may thus bias the inferred cosmology [e.g. 15, 16]. Another approach is to utilize analytic prescriptions to capture the modifications in dark matter halos through a set of baryonic parameters, these parameters can be calibrated from hydrodynamical simulations and/or varied alongside cosmology during the inference process. Examples of this approach include, HMCode which uses the halo model formalism to modify halo shapes and their baryonic content [1, 17], and the *baryonification* method which modifies particle positions in gravity-only simulations to emulate the impact of baryonic physics [18, 19]. Alternatively, the PCA method directly models the impact of baryonic feedback at the level of summary statistics by employing a set of eigenmodes and marginalizing over their amplitudes [20, 21].

State-of-the-art baryon mitigation techniques generally model the growth of structure and baryonic feedback independently despite the intrinsic link between galaxy formation and the underlying cosmology. Previous studies using hydrodynamical simulations have found that, for a given subgrid physics implementation, the suppression in the matter power spectrum varies with cosmological parameters [e.g. 19, 22–25]. Feedback effects are more pronounced in cosmologies where halos have a shallower gravitational potential well (e.g. due to changes in concentration) or higher baryon fractions [26]. While there is evidence that this coupling has negligible impact on cosmological constraints even for a *Euclid*-like survey [22, 27], these studies have been limited by the accuracy of the analytical fitting functions used for building mock data. Therefore, it is important to further investigate these effects in the context of Stage IV surveys which will push us deeper into the non-linear regime [28]. Note that the dependence of baryonic feedback on cosmology is distinct from the degeneracy between the two, the latter simply implies that their effects on observables are indistinguishable.

The goal of this work is to ascertain whether baryon mitigation techniques, which assume baryonic feedback to be independent of cosmology, can deliver unbiased cosmological constraints. In particular, we consider two such techniques: PCA [20, 21] and the HMCODE2020 model [1, 17]. The PCA method uses sets of hydrodynamical simulations to identify eigenmodes, also called principal components (PCs), which can be used to model the corrections due to baryons. These PCs are added to the dark matter-only data vector with their amplitude as free parameters. In contrast, the HMCODE2020 approach explicitly models the modification to the matter power spectrum through a halo model formalism with free parameters for baryonic feedback that are calibrated from simulations. Both these methods have been used for baryon mitigation in weak lensing analyses [e.g. 3, 29–31].

We characterize the performance of these methods using hydrodynamical simulations covering wide range of fiducial cosmologies. We build mock 3×2 pt data vectors using the *Magneticum* hydrodynamical simulation suite, which spans fifteen cosmologies. Using these mock data, we perform simulated likelihood analyses for a LSST Y1-like survey and quantify the parameter bias that arises from the coupling between cosmology and baryonic feedback.

This paper is organized as follows. In section 2 we describe the hydrodynamical simulations and their basic properties. In section 3 we discuss the suppression in the matter

	Ω_m	Ω_b	σ_8	h	Ω_b/Ω_m
C1	0.153	0.0408	0.614	0.666	0.267
C2	0.189	0.0455	0.697	0.703	0.241
C3	0.200	0.0415	0.850	0.730	0.208
C4	0.204	0.0437	0.739	0.689	0.214
C5	0.222	0.0421	0.793	0.676	0.190
C6	0.232	0.0413	0.687	0.670	0.178
C7	0.268	0.0449	0.721	0.699	0.168
C8 (WMAP7)	0.272	0.0456	0.809	0.704	0.168
C9	0.301	0.0460	0.824	0.707	0.153
C10	0.304	0.0504	0.886	0.740	0.166
C11	0.342	0.0462	0.834	0.708	0.135
C12	0.363	0.0490	0.884	0.729	0.135
C13	0.400	0.0485	0.650	0.675	0.121
C14	0.406	0.0466	0.867	0.712	0.115
C15	0.428	0.0492	0.830	0.732	0.115

Table 1: Cosmological parameter combinations for the 15 simulations in the *Magneticum* suite.

power spectrum measured from the *Magneticum* simulations. Section 4 details the theory model, analysis choices and survey design. We present the results in section 5 and analyze the performance of the baryon mitigation techniques across cosmologies. We conclude in section 6.

2 Simulations

2.1 Magneticum

The *Magneticum*⁴ suite of hydrodynamical simulations [32–38] were run using the smoothed particle hydrodynamics code P-GADGET3 [39]. The subgrid physics implementation in these simulations includes radiative cooling, heating, ultraviolet background, star formation [40]; stellar evolution, chemical enrichment, and metallicity dependent cooling [41, 42]; feedback from supernovae driven galactic winds and active galactic nuclei [32, 43].

Several studies have shown that the *Magneticum* simulations reproduce a wide range of observations spanning from galactic to cluster scales including: the galaxy stellar mass function [44]; AGN luminosity function [45]; properties of the intra-cluster medium (e.g. temperature profiles) [46, 47] and the Sunyaev-Zeldovich power spectrum [34]. Of particular relevance to this work is the baryon fraction in galaxy groups and clusters, a strong indicator of the strength of feedback [24, 48], which has also been found to be consistent with observations [49, 50]. The level of suppression in the matter power spectrum is similar to the BAHAMAS simulations [51].

In this work we use the multi-cosmology *Box3/hr* simulations that have a box size of 128 Mpc h^{-1} . The suite consists of 15 simulations C1, C2... C15, numbered in order of increasing Ω_m . Each simulation is run using a total of 2×576^3 particles with gas and dark matter mass

⁴<http://www.magneticum.org>

Simulation	Box Size (Mpc h^{-1})	Total Particles	Dark matter particle mass ($M_{\odot} h^{-1}$)	Initial gas particle mass ($M_{\odot} h^{-1}$)	Cosmology
Eagle	67.77	2×1504^3	6.57×10^6	1.23×10^6	<i>Planck2013</i>
IllustrisTNG	75	2×1820^3	5.06×10^6	9.44×10^5	<i>Planck2013</i>
Illustris	75	2×1820^3	4.41×10^6	8.87×10^5	<i>WMAP7</i>
MassiveBlack-II	100	2×1972^3	1.1×10^7	2.2×10^6	<i>WMAP7</i>
Horizon-AGN	100	2×1024^3	5.6×10^7	7×10^6	<i>WMAP7</i>
cosmo-OWLS	400	2×1024^3	3.75×10^9	7.54×10^8	<i>WMAP7</i>
BAHAMAS	400	2×1024^3	3.85×10^9	7.66×10^8	<i>WMAP9</i>

Table 2: Simulations used for PCA training.

resolutions of $m_{\text{gas}} = 1.4 \times 10^8 M_{\odot} h^{-1}$ and $m_{\text{DM}} = 6.9 \times 10^8 M_{\odot} h^{-1}$, respectively. The cosmological parameter combinations for the *Mangeticum* simulations are listed in table 1.

Out of these simulations, only C8, which is run at the fiducial *WMAP7* cosmology $\{\Omega_{\text{m}}, \Omega_{\text{b}}, \sigma_8, h, n_{\text{s}}\} = \{0.272, 0.0456, 0.809, 0.704, 0.963\}$ [52], is calibrated to reproduce observations. The remaining simulations adopt the same subgrid parameters, which ensures that any variations in feedback strength can be attributed solely to changes in cosmology.

2.2 Simulations for PCA training

We use an independent set of simulations for PCA training: Eagle [53], Illustris [54], IllustrisTNG [55], MassiveBlack-II [56], HorizonAGN [57], cosmo-OWLS [58], and BAHAMAS [51]. The latter two simulations include additional scenarios varying the strength of AGN feedback using the ΔT_{heat} parameter, which determines the amount of energy the black hole deposits to the neighboring gas particles. For cosmo-OWLS and BAHAMAS $\Delta T_{\text{heat}} = (10^{8.0}, 10^{8.5}, 10^{8.7})$ K and $(10^{7.6}, 10^{7.8}, 10^{8.0})$ K, respectively. The simulation characteristics are summarized in table 2.

These simulations cover a broad variety of subgrid physics implementations, e.g. Massive Black-II has relatively weak AGN feedback efficiency which results in an over-prediction of the abundance of massive galaxies at low redshifts [56], the violent radio mode AGN feedback in Illustris causes massive halos to be almost devoid of gas [59], and the AGN feedback in the Eagle simulation only injects energy through a thermal channel rather than the commonly used quasar- and radio-mode. As a result, the power spectrum suppression at $z = 0$ can vary up to 30% across these simulations along with different evolution with redshift – these variations ensure that the eigenmodes identified by the PCA have sufficient flexibility.

3 Impact of cosmology on baryonic feedback

The background cosmology dictates the hierarchical growth of dark matter halos, within which galaxies form and evolve. Primarily, the balance between the gravitational potential of a halo and the strength of feedback mechanisms determines the efficacy of baryonic feedback in redistributing matter [60, 61]. The resulting suppression in the matter power spectrum reflects the cumulative effect across the halo population. Consequently, variations in dark matter halo properties or the halo population itself, driven by changes in cosmology, can directly influence the effectiveness of feedback in altering the matter distribution.

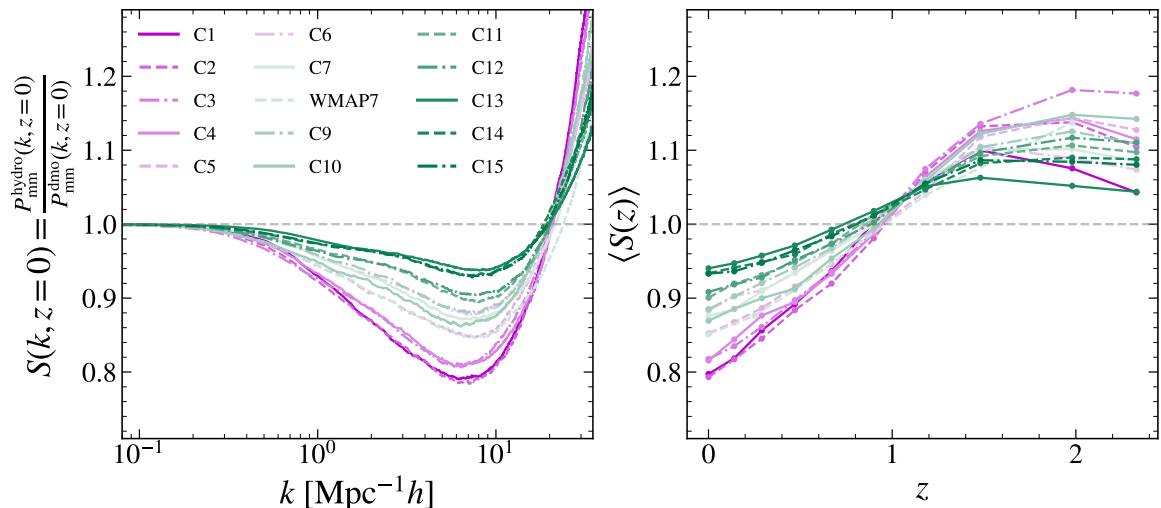


Figure 1: Suppression in the matter power spectrum for the *Magneticum* simulations. Left: Suppression as a function of wavenumber at $z = 0$. Right: Suppression averaged between $k = 1 - 10 \text{ Mpc}^{-1}h$ as a function of redshift.

For example, in less massive halos supernovae feedback is more important than AGN activity, while more massive halos, with their deeper potential wells, are less susceptible to AGN feedback [60–62]. As a result, changes in the halo abundance at a given mass (e.g. due to a different growth rate) can lead to a different level of suppression in the matter power spectrum. Halo concentration which has been found to depend on cosmology [63–65], also modulates the gravitational potential and affects the extent to which AGN feedback can expel gas. Furthermore, the cosmic baryon fraction influences the gas content of halos and thus impacts the reservoirs available to fuel AGN activity.

[26] explored several such mechanisms using the suppression in halo mass — the ratio of halo mass in the hydrodynamical and dark matter-only simulation — as a proxy. Specifically, they investigate the impact of halo concentration, formation epoch, and environment using the FLAMINGO suite of hydrodynamical simulations [66]. They find that for massive halos ($> 10^{13} M_{\odot}$), a higher concentration leads to smaller baryonic suppression due to the increased gravitational binding energy whereas in the low mass regime ($< 5 \times 10^{12} M_{\odot}$) this trend reverses. The trend for low mass halos is a result of concentration being anti-correlated with the formation epoch. Halos that form earlier are more concentrated but also have a larger black hole mass. For low mass halos, the non-linear black hole growth (as opposed to self-regulating black holes found in higher mass halos) makes AGN outflows more effective at expelling gas despite a higher concentration. They do not find any correlation between the suppression in halo mass and halo environment, which implies that the cosmology variations do not regulate feedback through this channel.

To demonstrate the impact of cosmological variations, figure 1 shows the suppression in the matter power spectrum from the *Magneticum* simulations at 15 different cosmologies. The suppression $S(k, z)$ is defined as

$$S(k, z) = \frac{P_{\text{mm}}^{\text{hydro}}(k, z)}{P_{\text{mm}}^{\text{dmo}}(k, z)}, \quad (3.1)$$

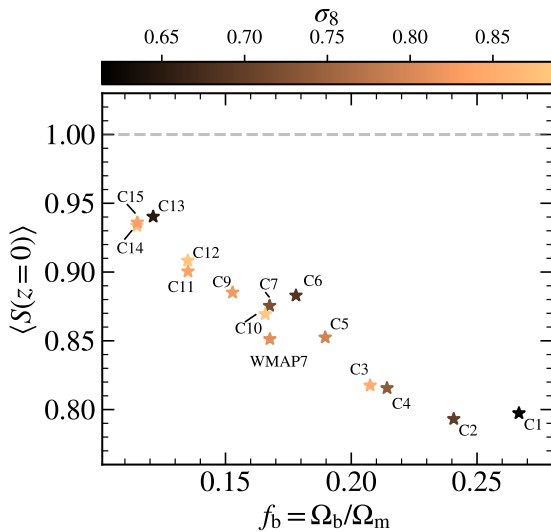


Figure 2: Average suppression in the power spectrum at $z = 0$ as a function of the baryon fraction. Overall we see that the suppression is primarily determined by the baryon fraction. C14 and C15 offset vertically for visual clarity.

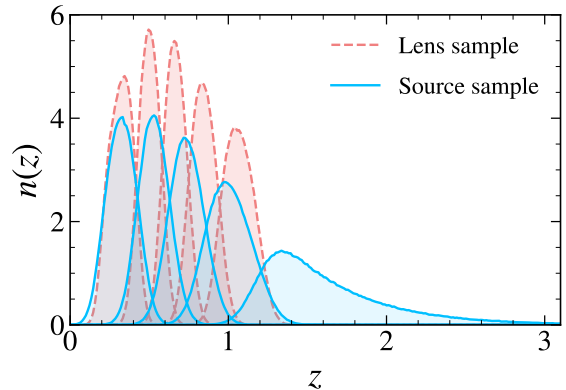


Figure 3: Normalized redshift distributions for LSST Y1. Refer to section 4.5 for details.

where $P_{\text{mm}}^{\text{hydro}}(k)$ and $P_{\text{mm}}^{\text{dmo}}(k)$ are the matter power spectra from hydrodynamical and dark matter-only simulations, respectively, for a given cosmology. The results in the left panel show that, even for the same subgrid physics, the strength of baryonic feedback can vary up to 15% for the cosmology variations considered here. In the right panel we show for each cosmology, the average suppression as a function of redshift, defined as

$$\langle S(z) \rangle = \frac{\int k^3 S(k, z) dk}{\int k^3 dk}, \quad (3.2)$$

where the lower and upper integration limits are $k = 1$ and $10 \text{ Mpc}^{-1}h$, respectively. We see that the evolution of baryonic feedback with redshift varies across cosmologies. For example, cosmologies C3 and C4 exhibit similar levels of suppression at $z = 0$, but differ by approximately 6% at $z = 2$. Overall, we see that scenarios with stronger suppression also exhibit a stronger evolution with redshift. Accurate modeling of these redshift evolution features might help in breaking degeneracies between cosmology and baryonic feedback processes.

To explore trends in feedback strength across cosmologies, figure 2 presents the average suppression as a function of the cosmic baryon fraction $f_b = \Omega_b / \Omega_m$. We find a strong correlation between suppression in the matter power spectrum and f_b . This correlation can be attributed to dark matter halos having larger gas reservoirs for fueling AGN activity. The strong dependence on f_b , even when multiple cosmological parameters are varied simultaneously, implies that the baryon fraction plays a dominant role in influencing feedback strength. These findings are consistent with previous results [see, e.g., Fig. 2 in 22], which show that the strength of baryonic effects primarily depends on f_b . We also find that other cosmological parameters, such as σ_8 and h , can have a weak but albeit discernible influence.

For example, C1 ($f_b = 0.267$) has a cosmic baryon fraction 10% larger than C2 ($f_b = 0.241$) and yet displays the same level of suppression. Similarly, C7 and WMAP7 have the same value of f_b and yet display a 2% variation in power spectrum suppression.

4 Simulated likelihood analysis

We perform simulated likelihood analyses using the standard LSST Y1 model implemented in COCOA⁵ [67], the latter integrates the theoretical modeling from COSMOLIKE [68] and the COBAYA framework [69]. We build mock data vectors at different cosmologies by using the power spectrum suppression measured from the *Magneticum* simulations. The data vector comprises the 2pt correlation functions of cosmic shear, galaxy-galaxy lensing, and galaxy clustering.

We now review the modeling ingredients for the simulated analyses including the computation of theory and mock data vectors, baryon mitigation techniques, and survey design.

4.1 Theory data vector

We compute the 2pt correlation functions from the projected angular power spectrum, the latter is computed using the Limber approximation and adopting a flat sky geometry. For two fields A and B , the angular power spectrum in the tomographic bin (i, j) is calculated from the 3D power spectrum P_{AB} as

$$C_{AB}^{ij}(\ell) = \int_0^{\chi_h} d\chi \frac{q_A^i(\chi) q_B^j(\chi)}{\chi^2} P_{AB}^{ij} \left(\frac{\ell + 1/2}{\chi}, \chi \right), \quad (4.1)$$

where $q^i(\chi)$ is the weight kernel, χ is the comoving distance, and χ_h is the comoving horizon distance. The weight kernels for the lensing convergence field κ and the galaxy density field δ_g are given by

$$q_{\kappa}^i(\chi) = \frac{3H_0^2 \Omega_m}{2c^2} \frac{\chi}{a(\chi)} \int_{\chi}^{\chi_h} d\chi' \frac{dz}{d\chi'} \frac{n^i(\chi')}{\bar{n}^i} \frac{\chi' - \chi}{\chi'}, \quad (4.2)$$

$$q_{\delta_g}^i(\chi) = \frac{n^i(\chi)}{\bar{n}^i} \frac{dz}{d\chi}, \quad (4.3)$$

where $n^i(\chi'(z))$ is the galaxy redshift distribution and a is the scale factor. The 3D power spectra for the fields read

$$P_{\kappa\kappa}^{ij}(k, z) = P_{\text{mm}}(k, z), \quad (4.4a)$$

$$P_{\delta_g\kappa}^{ij}(k, z) = b^i P_{\text{mm}}(k, z), \quad (4.4b)$$

$$P_{\delta_g\delta_g}^{ij}(k, z) = b^i b^j P_{\text{mm}}(k, z), \quad (4.4c)$$

where b^i is the linear galaxy bias and $P_{\text{mm}}(k, z)$ is the non-linear matter power spectrum computed from CAMB [70]. The 3D power spectra in equations 4.4a, 4.4b & 4.4c are converted to angular power spectra using eq. 4.1, from which the 2pt correlation functions

⁵<https://github.com/CosmoLike/cocoa>

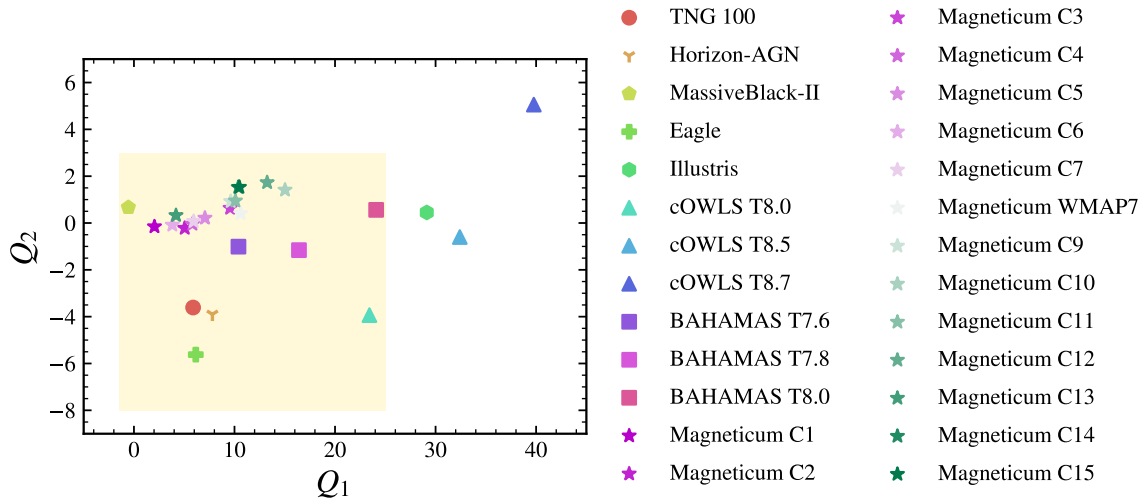


Figure 4: Amplitudes of the first two principal components measured from hydrodynamical simulations. The amplitudes are estimated by projecting the mock data vector on the PCs, as the latter form an orthogonal basis. The mock data vectors for *Magneticum* simulations are computed at their respective cosmologies while the mock data vector for the remaining simulations assume a *WMAP7* cosmology. The shaded region represents the informative prior used in the analysis, see Sec. 4.6.1 for details.

for cosmic shear $\xi_{\pm}(\theta)$, galaxy-galaxy lensing $\gamma_t(\theta)$, and galaxy clustering $w(\theta)$ are computed as

$$\xi_{\pm}^{ij}(\theta) = \sum_{\ell} \frac{2\ell + 1}{2\pi\ell^2(\ell + 1)^2} \left[G_{\ell,2}^{+}(\cos\theta) \pm G_{\ell,2}^{-}(\cos\theta) \right] C_{\kappa\kappa}^{ij}(\ell), \quad (4.5)$$

$$\gamma_t^{ij}(\theta) = \sum_{\ell} \frac{(2\ell + 1)}{2\pi\ell^2(\ell + 1)^2} P_{\ell}^2(\cos\theta) C_{\delta_g\kappa}^{ij}, \quad (4.6)$$

$$w^i(\theta) = \sum_{\ell} \frac{2\ell + 1}{4\pi} P_{\ell}(\cos\theta) C_{\delta_g\delta_g}^{ii}(\ell), \quad (4.7)$$

where P_{ℓ} and G_{ℓ}^{\pm} are the Legendre and associated Legendre polynomials, respectively [cf. 71].

4.2 Systematics

We include the following systematic effects

- *Intrinsic alignments:* Intrinsic alignments (IA) contaminate the measured cosmic shear signal by introducing additional correlations between galaxy shapes. We model the IA contribution using a redshift dependent non-linear alignment (NLA) model [72] parametrized by the amplitude a_{IA} and redshift evolution η_{IA}

$$A_{\text{IA}}(z) = -a_{\text{IA}} \frac{C_1 \rho_{\text{crit}} \Omega_{\text{m}}}{G(z)} \left(\frac{1+z}{1+z_{0,\text{IA}}} \right)^{\eta_{\text{IA}}}, \quad (4.8)$$

where, $C_1 \rho_{\text{crit}} = 0.0134$, $z_{0,\text{IA}} = 0.62$, Ω_{m} is the matter density, and $G(z)$ is the linear growth factor.

- *Photometric redshifts*: The uncertainty in the redshift distribution $n^i(z)$ is modeled by including a parameter Δz^i for each tomographic bin which shifts the distribution as

$$n^i(z) \rightarrow n^i(z + \Delta z^i). \quad (4.9)$$

We use separate shift parameters Δz_{lens}^i and $\Delta z_{\text{source}}^i$ for the lens and source samples, respectively.

- *Shear calibration bias*: Galaxy shapes are biased estimators of the underlying shear and the response of the shear estimator has to be calibrated. The residual biases in the shear calibration in a tomographic bin are quantified by the multiplicative calibration bias m^i .
- *Galaxy bias*: We assume linear galaxy bias when modeling the galaxy-galaxy lensing and galaxy clustering parts of the data vector. In total we have five galaxy bias parameters b^i , one for each tomographic bin.

4.3 Baryon mitigation techniques

We test two methods for modeling baryonic effects.

- **PCA**: The PCA method [20, 21] uses the difference between the mock data vectors from simulations and theory predicted data vectors, where each data vector consists of $(\xi_{\pm}(\theta), \gamma_t(\theta), w(\theta))$, to identify principal components. These PCs serve as a flexible basis for modeling baryonic effects on smaller scales. For details about the computation of principal components we refer the reader to [21]. Note that the *Magneticum* simulations, which are used for computing mock data vectors, do not enter PCA training. The model prediction $\mathbf{D}_{\text{model}}$ is given as the of sum the theory data vector $\mathbf{D}_{\text{theory}}$ and the principal components \mathbf{P}_i weighted by amplitudes Q_i

$$\mathbf{D}_{\text{model}} = \mathbf{D}_{\text{theory}} + \sum_{i=1}^N Q_i \mathbf{P}_i, \quad (4.10)$$

where N is the number of principal components. The theory data vector is generated using the non-linear matter power spectrum from HALOFIT [73] following the procedure in section 4.1. The PC amplitudes Q_i are treated as free parameters, which allows us to marginalize over baryonic scenarios during cosmological inference.

The PCA is trained using a difference matrix that depends on both theoretical and mock data vectors. Consequently, the resulting eigenmodes are sensitive to the cosmology at which these data vectors are computed. To train the PCA, we adopt the *WMAP7* cosmology [52] as the baseline for two key reasons: (i) approximately half of the simulations used for PCA training (described in section 2.2) are run at this cosmology, and (ii) the *Magneticum C8* simulation is also run at this exact cosmology which allows us to evaluate the PCA’s ability to capture the subgrid physics implemented in *Magneticum*.

The galaxy clustering and galaxy-galaxy lensing parts of the data vector are robust to baryonic feedback due to the choice of scale cuts (cf. section 4.5). Therefore, the principal components only apply corrections to cosmic shear.

- **HMCODE2020:** The HMCODE2020 (hereafter, HM20) framework takes a halo model approach to model the effects of non-gravitational physics on the matter power spectrum [1, 17]. The model comprises parameters that govern the change in the internal structure of dark matter halos, specifically, the modification in halo concentration (B), the formation of stars which dominate the matter profile in the halo centers (f_*), and the expulsion of gas from halos (M_b). These parameters are calibrated using the power spectrum response from the BAHAMAS *WMAP9* simulations for wavenumbers in the range $k = 0.3$ to $20 \text{ Mpc}^{-1}h$ at $z < 1$. HM20 is able to match the measurements from the simulation upto a few percent in the fitted range. In the commonly used single parameter variant of HM20, the model parameters are expressed as a function of the AGN feedback strength $\Theta_{\text{AGN}} \equiv \log(T_{\text{AGN}}/\text{K})$, here, T_{AGN} is related to the heating temperature of gas particles when an AGN feedback event occurs.

For generating the model data vector with HM20, we evaluate the equations in section 4.1 using the `mead2020_feedback` option in CAMB.

4.4 Mock data

To build mock data vectors at different cosmologies which are *contaminated* by baryonic effects, we use the power spectrum suppression inferred from the *Magneticum* simulations and modify the theoretical prediction (e.g. from HALOFIT) which does not model these effects. For a simulation at a cosmology θ_{sim} , we compute the power suppression $S(k, z)$ as a function of wavenumber k and redshift z by taking the ratio of the matter power spectrum from the hydrodynamical simulation and its dark matter-only counterpart (equation 3.1). We use $S(k, z|\theta_{\text{sim}})$ to modify the theory prediction of the non-linear matter power spectrum, P_{mm} , as

$$P_{\text{mm}}(k, z|\theta_{\text{sim}}) \rightarrow S(k, z|\theta_{\text{sim}}) \times P_{\text{mm}}(k, z|\theta_{\text{sim}}). \quad (4.11)$$

For the PCA method, we compute P_{mm} using the HALOFIT option in CAMB. For HM20, however, the `mead2020_feedback` model which applies baryonic corrections and is parameterized by Θ_{AGN} , does not recover the dark matter-only prediction under any limit of Θ_{AGN} . Therefore, we compute the mock data vector for HM20 by modifying P_{mm} from the `mead2020` option. We then proceed to compute mock data using the contaminated matter power spectrum and following the modeling recipe described in section 4.1.

4.5 Survey Design

We perform a simulated LSST Y1 analysis, following the survey design outlined in the DESC Science Requirements Document (DESC SRD, [74]). The analysis assumes a survey area of $12,300 \text{ deg}^2$, with redshift distributions for the lens and source samples derived using limiting i -band magnitudes of 24.1 and 25.1, respectively. The redshift distributions are modeled using the analytical form $n(z) \propto z^2 \exp[-(z/z_0)^\alpha]$. For the lens sample, we set $(z_0, \alpha) = (0.26, 0.94)$ and normalize the distribution by an effective number density $n_{\text{eff}} = 18 \text{ arcmin}^{-2}$. The sample is then divided into five equally populated tomographic bins (differing from the DESC SRD, which uses 10 bins) based on estimated redshift and each bin is convolved with a Gaussian photo- z scatter of $\sigma_z = 0.03(1+z)$. For the source sample, we use $(z_0, \alpha) = (0.19, 0.87)$ and normalize the distribution to $n_{\text{eff}} = 11.2 \text{ arcmin}^{-2}$. The source sample is also split into five tomographic bins, with each bin convolved with a Gaussian photo- z uncertainty of $\sigma_z = 0.05(1+z)$. The lens and source redshift distributions are shown in figure 3.

Parameter	Prior		Fiducial Value
Cosmology			
A_s	Flat	$(5 \times 10^{-10}, 1 \times 10^{-8})$	Varied
Ω_m	Flat	$(0.05, 0.9)$	Varied
$\omega_b \equiv \Omega_b h^2$	Gaussian	$(\omega_b^{\text{fid}}, 0.0016)$	Varied
h	Flat	$(0.55, 0.91)$	Varied
n_s	Flat	$(0.87, 1.07)$	0.963
Σm_ν	Fixed		0.06 eV
Photo-z shift			
Δz_{lens}^i	Gaussian	$(0.0, 0.005)$	0.0
$\Delta z_{\text{source}}^i$	Gaussian	$(0.0, 0.002)$	0.0
Linear galaxy bias			
b^i	Flat	$(0.8, 3)$	$[1.24, 1.36, 1.47, 1.60, 1.76]$
Shear calibration			
m^i	Gaussian	$(0.0, 0.005)$	0.0
Intrinsic Alignment			
A_{IA}	Flat	$(-5, 5)$	0.5
η_{IA}	Flat	$(-5, 5)$	0.0
Baryon Model: PCA			
Q_1	Flat	$(-1, 25)$	-
Q_2	Flat	$(-8, 3)$	-
Baryon Model: HM20			
$\Theta_{\text{AGN}} \equiv \log_{10}(T_{\text{AGN}}/\text{K})$	Flat	$(7, 8)$	-

Table 3: Model parameters and priors for the simulated likelihood analyses. Flat(a, b) denotes a flat prior within lower and upper limits a and b , respectively. Gaussian(μ, σ) denotes a Gaussian prior with mean μ and standard deviation σ . The fiducial values for cosmology parameters are enumerated in table 1.

Following the DESC SRD, we choose a scale cut of $k_{\text{max}} = 0.3 \text{ Mpc}^{-1} h$, which approximately corresponds to a minimum comoving scale $R_{\text{min}} = 2\pi/k_{\text{max}} = 21 \text{ Mpc } h^{-1}$. For galaxy clustering, the angular scale cut for a tomographic bin i is $\theta_{\text{min}}^i = R_{\text{min}}/\chi(\bar{z}^i)$, where \bar{z}^i is the mean redshift of the tomographic bin. Thus for the lens sample, the minimum comoving scale translates to angular scale cuts of $[105.86', 81.17', 71.24', 65.32', 61.49']$; we adopt the same angular scale cuts for galaxy-galaxy lensing. For cosmic shear, we restrict the analysis to an angular multipoles of $\ell < \ell_{\text{max}} = 5000$, which is more aggressive than the scale cut of $\ell_{\text{max}} = 3000$ specified in the DESC SRD. The angular scale cuts for the correlation functions ξ_{\pm} are determined by the first zeros of their corresponding spherical Bessel function $J_{0/4}(\ell\theta)$, which translates to a minimum angular scales of $\theta_{\text{min}}^{\xi_{+}} = 2.4048/\ell_{\text{max}} = 1.653'$ and $\theta_{\text{min}}^{\xi_{-}} = 7.5883/\ell_{\text{max}} = 5.217'$.

Note that as a consequence of the scale cuts described above, the galaxy clustering and galaxy-galaxy lensing data vectors are robust to baryonic effects and thus the constraints on baryonic feedback parameters are driven by cosmic shear data only.

4.6 Likelihood and covariance

We use the Python package EMCEE [75] to sample the posterior distribution assuming a Gaussian likelihood

$$\log \mathcal{L} = -\frac{1}{2}(\mathbf{D}_{\text{mock}} - \mathbf{D}_{\text{model}})^T \mathbf{C}^{-1}(\mathbf{D}_{\text{mock}} - \mathbf{D}_{\text{model}}), \quad (4.12)$$

where \mathbf{C} and \mathbf{D} refer to the covariance and data vector, respectively, and the subscript denotes if the latter is the mock or the model data vector. We use a Gaussian prior on the physical baryon density $\Omega_b h^2$ with the prior width set to ten times the measurement uncertainty from *Planck* [2]. The model parameters priors are summarized in Table 3.

The covariance for the 3×2 pt data vector is calculated using the publicly available code COSMOCOV⁶ [76] which is built upon the COSMOLIKE framework. COSMOCOV uses the 2D-FFTLog algorithm to efficiently compute real-space covariance matrices. We compute the cosmic shear covariance which consists of Gaussian, super-sample covariance and connected non-Gaussian components.

Since the model data vector evaluations are slow and computationally expensive, we use the neural network emulator presented in [77] which predicts the model data vector as function of cosmology and nuisance parameters. We train separate emulators for each component of the data vector $(\xi_+, \xi_-, \gamma_t, w)$. As the fiducial cosmologies for the *Magneticum* simulations differ significantly, we train separate emulators for each cosmology to ensure prediction accuracy. We refer the reader to [77] for further details about the emulator architecture and training method.

4.6.1 Prior on baryonic feedback parameters

The simulations used for constructing the PC basis can serve as external information to inform priors that better match observations. Figure 4 shows the distribution of the PC amplitudes $\{Q_i\}$ for the simulations considered in this work⁷. We derive informative priors for the PC amplitudes by examining the range of $\{Q_i\}$ spanned in the figures (not including the *Magneticum* simulations), as indicated by the shaded region. We exclude the Illustris, cOWLS T8.5, and cOWLS T8.7 simulations when determining these priors as they represent too extreme feedback scenarios. The baryon fractions in group and cluster sized halos predicted by the Illustris simulation are in disagreement with observations due to the strong AGN radio-mode feedback [59, 78]. The cOWLS T8.5 and cOWLS T8.7 simulations also do not reproduce the observed gas fractions in massive halos [79].

5 Results

5.1 Performance at the baseline *WMAP7* cosmology

We first assess the performance of the baryon mitigation techniques in capturing the baryonic feedback in the *Magneticum WMAP7* (C8) simulation. Note that, while the principal components are computed at the *WMAP7* cosmology, the *Magneticum* simulations are not used for training the PCA. Similarly, HM20 is calibrated on the BAHAMAS *WMAP9* simulation

⁶<https://github.com/CosmoLike/CosmoCov>

⁷The amplitudes for each simulations are estimated by projecting the difference between the mock and theory data vectors onto the principal eigenmodes. Since the PCs form an orthogonal basis, by construction, the amplitude is simply $Q_i = \frac{1}{\|\mathbf{P}_i\|} \mathbf{P}_i^T (\mathbf{D}_{\text{mock}} - \mathbf{D}_{\text{theory}})$

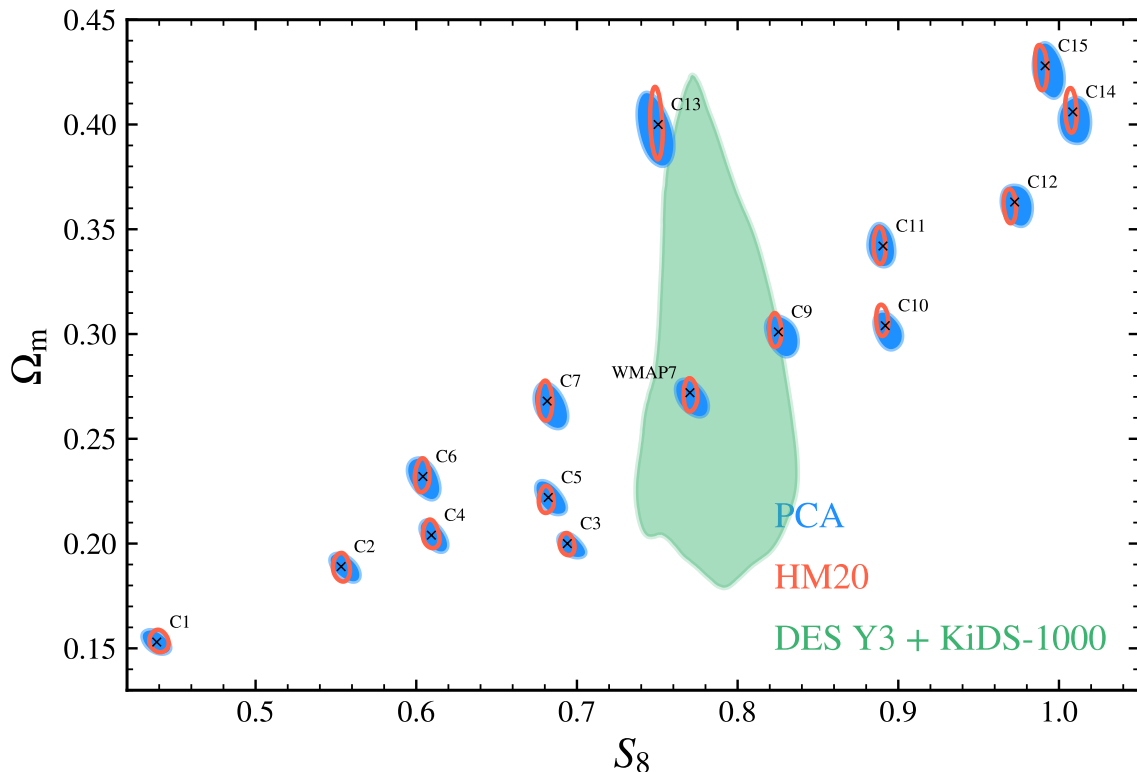


Figure 5: Results from simulated 3×2 pt analysis as a function of cosmology. The figure shows 1σ contours (39.35% credible intervals) in Ω_m – S_8 when a mock data vector contaminated by baryonic effects is fit using PCA and HM20. At each cosmology, we compute the mock data vector by modifying the non-linear matter power spectrum by the suppression measured from the *Magneticum* simulation. The cross marker represents the true values (refer to table 1 for list of parameter values at the 15 cosmologies). For reference we also show 3σ contours (98.9% credible intervals) from the joint DES Y3 + KiDS 1000 analysis [31]. Note that the constraints shown in this figure include projection effects, however, they’re insignificant at the scale of this visualization.

which differs from *Magneticum* in its subgrid physics implementation. Therefore, it is important to first verify if both methods result in unbiased inference at this baseline scenario before considering variations in cosmology.

For a quantitative assessment of the performance of the two methods, we adopt the bias in the Ω_m – S_8 plane as our metric, as the two parameters are of key interest for weak lensing surveys. We consider the baryon model to be effective if the bias in the 2D marginalized mean is below 0.3σ . The bias in mean parameter values can also result from the marginalization in the high dimensional parameter space. To account for these so-called projection effects, we repeat the analysis by fitting a data vector generated from the model and adopt the resulting 2D marginalized mean as the reference, rather than the fiducial parameter values, for computing the bias⁸. Using the same model for, both, generating and fitting the data vector

⁸The bias is computed as $\frac{\text{bias}}{\sigma} = \sqrt{\mathbf{X}^T \mathbf{C}_{\Omega_m-S_8}^{-1} \mathbf{X}}$, where $\mathbf{X} = (\Delta\Omega_m, \Delta S_8)^T$ is the difference between the 2D marginalised mean and the *reference* parameter values. $\mathbf{C}_{\Omega_m-S_8}$ is the marginalized parameter covariance

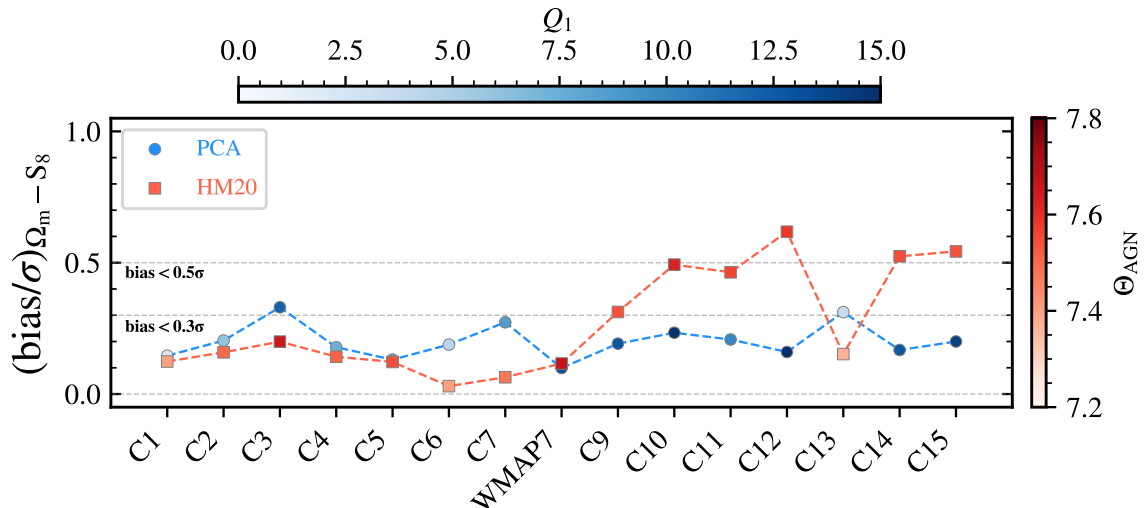


Figure 6: Bias in $\Omega_m - S_8$ at different cosmologies when using PCA and HM20 to mitigate baryonic effects. The marker color represents the amplitude of baryonic feedback parameter in the respective models, Q_1 for PCA and Θ_{AGN} for HM20. The bias when using PCA is $< 0.3\sigma$ (0.5σ) in 13 (all) scenarios indicating that that PCA is robust to the coupling between baryonic feedback and cosmology, meanwhile, using HM20 results in $< 0.3\sigma$ (0.5σ) bias for 9 (12) scenarios. The bias shown here is corrected for projection effects.

eliminates model misspecification and isolates the bias due to projection effects, enabling us separate it from the systematic effect of interest.

The two baryon models exhibit comparable accuracy in the 3×2 pt analysis at the baseline cosmology. For PCA and HM20, we recover cosmological parameters within 0.1σ and 0.12σ , respectively, indicating that both methods effectively capture the subgrid physics implementation in *Magneticum*. Therefore, any bias observed when repeating the analysis for other cosmologies would therefore arise from variations in cosmology and the resulting modulation of suppression in the matter power spectrum.

5.2 Baryon mitigation across cosmologies

After validating both methods at the baseline cosmology, we perform simulated analysis at the remaining cosmological scenarios. In figure 5, we show the $\Omega_m - S_8$ constraints across the 15 cosmologies using PCA in blue and HM20 in red. The estimated bias at each cosmology is shown in figure 6, where we also color the symbol based on baryonic feedback parameter i.e. Q_1 for PCA and Θ_{AGN} for HM20. We find that the PCA method obtains unbiased parameter constraints in all but two scenarios. The parameter bias is at most weakly correlated with feedback strength, as measured by the first PC amplitude⁹. While relaxing the priors on PC amplitudes results in a loss of constraining power, it also makes it more robust to such effects. When using flat wide priors of $(-50, 50)$, the bias is $< 0.3\sigma$ in all cases. The HM20 model

in the $\Omega_m - S_8$ plane.

⁹While Q_1 represents the level of suppression in the data vector, the values at different cosmologies must be interpreted with caution. This is because Q_1 is proportional to the absolute change in the data vector, as evident from equation 4.10; therefore cosmologies with larger Ω_m or σ_8 (and hence larger $P_{\text{mm}}(k)$ amplitude) will naturally have larger Q_1 even if the suppression is relatively small.

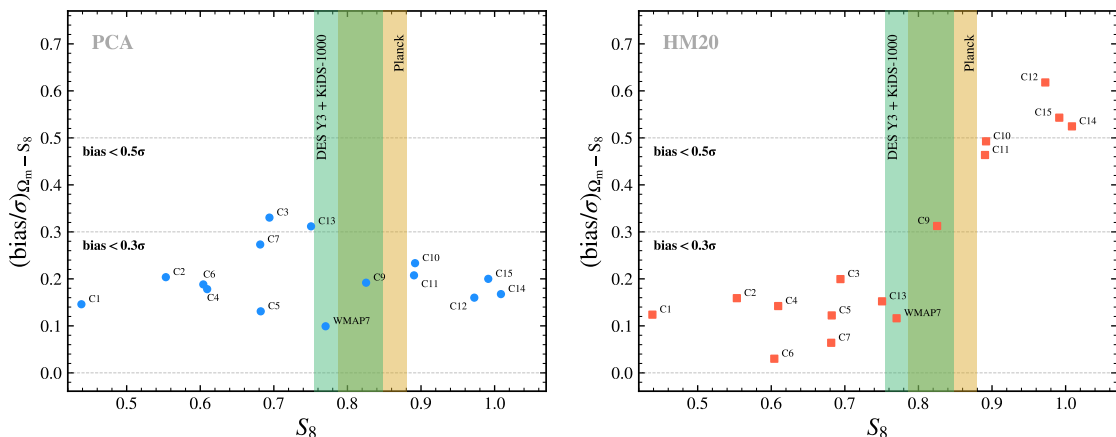


Figure 7: Bias in $\Omega_m - S_8$ as a function of S_8 . Results for PCA and HM20 model are shown in the left and right panels, respectively. The shaded regions represent 3σ (99.7% confidence levels) constraints from DES Y3 + KiDS-1000 analysis [31] and *Planck* [2]. We do not find a significant trends for PCA, while the bias for HM20 shows strong correlation with the input cosmology. Note that the parameter bias shown here is corrected for projection effects.

results in biased constraints at six out of the fifteen cosmologies and in three scenarios the bias is $> 0.5\sigma$. Note that, neither PCA or HM20 are trained/calibrated on the *Magneticum* simulations

The bias when using the HM20 model correlates with the input cosmological parameters (most notably S_8) while we do not observe any such trend for PCA, as shown in figure 7. For comparison, we show 3σ constraints from the DES Y3 + KiDS-1000 analysis [31] and *Planck* [2] as shaded regions. Even when considering only the cosmologies that are feasible given the constraining power of existing surveys, these results suggests that the bias induced due to a coupling with cosmology can still be significant for HM20. This implies that HM20 may not fully capture the impact of cosmology on feedback strength at LSST Y1 accuracy. This is corroborated by previous findings that the HM20 model calibrated using the BAHAMAS *WMAP9* simulation shows differences of a few percent when it is used to predict the suppression in BAHAMAS *Planck2013* simulation [see Sec. 6.3 in 1]. Another possibility is that the HM20 predictions get progressively inaccurate at higher redshifts as the model is calibrated only at $z < 1$.

One way to enhance the performance of HM20 is to introduce greater model flexibility. Instead of parameterizing in terms of the subgrid heating temperature, Θ_{AGN} , we can directly fit the model parameters (B, f_*, M_b) along with their redshift dependence. While this approach may introduce parameter degeneracies, applying informative priors based on simulations can mitigate this issue. For example, [1] provides priors derived from fits to the BAHAMAS and cosmo-OWLS simulations. Additionally, exploring alternative parameterizations of redshift evolution could improve accuracy, as [1] found that the power-law z -dependence adopted in HM20 led to inaccurate fits for $z > 1$. The performance of PCA is also dependent on the simulation set used for training and the prior on PC amplitudes, therefore the precision is likely to improve as more realistic simulations are included in the training set.

We repeat the simulated analyses using only the cosmic shear component of the data

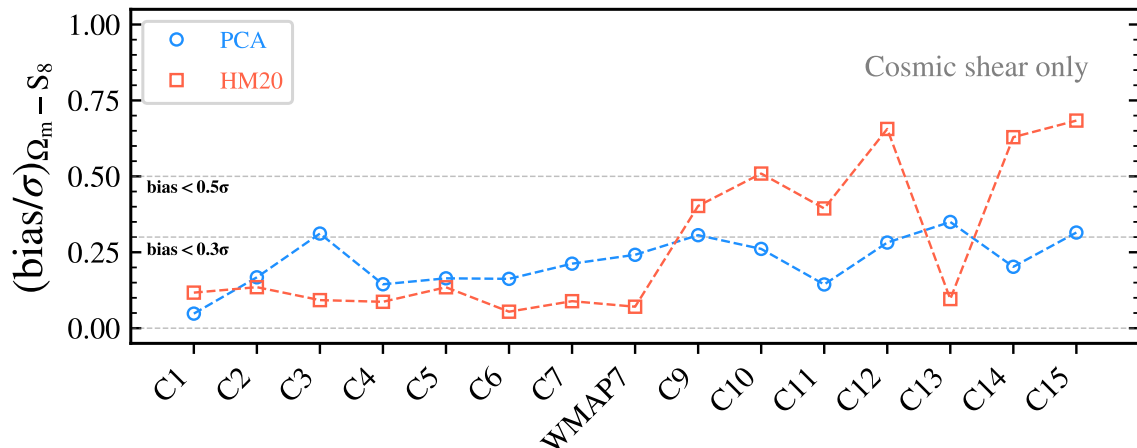


Figure 8: Bias in $\Omega_m - S_8$ when analyzing a cosmic shear only data vector, corrected for projection effects. The bias for both baryon mitigation methods is larger compared to the 3×2 pt case (figure 6).

vector and observe a degradation in the performance for both PCA and HM20, as shown in figure 8. While the galaxy clustering and galaxy-galaxy lensing portions of our data vector are insensitive to baryonic feedback due to the scale cuts applied, including probes such as the Sunyaev-Zeldovich effects, which incorporate both cosmological and astrophysical information, can help disentangle parameter degeneracies and mitigate the impact of the coupling [80].

6 Conclusions

Stage IV surveys will deliver vast volumes of data, enabling an unprecedented level of precision in cosmological measurements and inference. To fully leverage the statistical power of these datasets, these advances in data acquisition must be matched by improvements in modeling techniques. Of particular importance is understanding the growth of structure on non-linear scales. In the context of weak lensing analyses, the modeling uncertainty on small scales is dominated by baryonic processes like stellar and AGN feedback.

Current analyses generally assume the impact of baryonic feedback on the matter distribution to be independent of the underlying cosmology. We test this assumption and quantify its impact on parameter inference using the *Magneticum* suite of hydrodynamical simulations. These simulations are run at a fixed calibration of subgrid physics parameters which allows us to isolate the dependence of baryonic feedback on cosmology. We find that the suppression in the matter power varies up to 15% across the cosmologies spanned by the simulations. We show that the suppression in the power spectrum is primarily determined by the cosmic baryon fraction $f_b = \Omega_b/\Omega_m$ with other cosmological parameters resulting in a few percent effect at most.

We generate mock 3×2 pt data vectors by modifying the non-linear matter power spectrum with the suppression measured from the 15 *Magneticum* simulations. We test two baryon mitigation techniques, PCA and HM20, by performing a simulated analyses for a LSST Y1 like survey. Our analysis shows that the PCA method is robust to cosmologi-

cal variations, while HM20 exhibits a bias greater than 0.3σ in Ω_m-S_8 at six out of fifteen cosmologies.

For the PCA method, we do not observe significant correlation between the bias and either feedback strength or the fiducial cosmology, suggesting that PCA effectively captures these features. We find that the bias in parameter inference from the HM20 model is correlated with the background cosmology. This indicates that the dependence on cosmology assumed in HM20 (through the cosmic baryon fraction) might not be sufficiently accurate and needs further investigation. As the redshift evolution of feedback strength also changes with cosmology, the performance of HM20 might also be limited by the redshift evolution of parameters assumed in the model. To improve model flexibility, one approach is to relax current assumptions by introducing additional parameters and/or allowing existing parameters to vary independently, rather than being tied to Θ_{AGN} . Advancements in hydrodynamical simulations will be crucial for enhancing the performance of both baryon mitigation techniques. Simulations suites such as ANTILLES [48] and FLAMINGO [66] span wider range of possible feedback scenarios and can thus be used to determine realistic priors for model parameters.

In conclusion, cosmological inference at the precision required for upcoming surveys will demand a thorough evaluation of baryon modeling. It is essential to rigorously test these models using mock datasets from hydrodynamical simulations. Since the sensitivity to the coupling between cosmology and baryonic feedback is likely influenced by subgrid physics parameters, the performance of baryon models must be assessed across data vectors that span a range of cosmologies and feedback implementations.

Acknowledgments

We thank Tiago Castro for assistance with the Magneticum measurements and insightful discussions during the initial stages of this work. PRS also thanks Shivam Pandey for helpful discussions. PRS is supported in part by a Joint Fellowship Program between the University of Arizona and CNRS. PRS and EK are supported in part by Department of Energy grant DE-SC0020247 and the David and Lucile Packard Foundation. KD acknowledges support by the COMPLEX project from the European Research Council (ERC) under the European Union’s Horizon 2020 research and innovation program grant agreement ERC-2019-AdG 882679 as well as by the Deutsche Forschungsgemeinschaft (DFG, German Research Foundation) under Germany’s Excellence Strategy - EXC-2094 - 390783311. The calculations for the hydrodynamical simulations were carried out at the Leibniz Supercomputer Center (LRZ) under the project pr83li (Magneticum). KB, EA, and YD received funding from the Centre National d’Etudes Spatiales for the completion of this work. The analyses in this work were carried out using the High Performance Computing (HPC) resources supported by the University of Arizona Technology and Research Initiative Fund (TRIF), University Information Technology Services (UITS), and the office for Research, Innovation, and Impact (RDI) and maintained by the UA Research Technologies Department.

References

- [1] A.J. Mead, S. Brieden, T. Tröster and C. Heymans, *HMCODE-2020: improved modelling of non-linear cosmological power spectra with baryonic feedback*, *Monthly Notices of the Royal Astronomical Society* **502** (2021) 1401 [2009.01858].

- [2] Planck Collaboration, N. Aghanim, Y. Akrami, M. Ashdown, J. Aumont, C. Baccigalupi et al., *Planck 2018 results. VI. Cosmological parameters*, *Astronomy and Astrophysics* **641** (2020) A6 [1807.06209].
- [3] M. Asgari, C.-A. Lin, Joachimi, Benjamin, Giblin, Benjamin, Heymans, Catherine, Hildebrandt, Hendrik et al., *Kids-1000 cosmology: Cosmic shear constraints and comparison between two point statistics*, *A&A* **645** (2021) A104.
- [4] S. Alam, M. Aubert, S. Avila, C. Balland, J.E. Bautista, M.A. Bershadsky et al., *Completed SDSS-IV extended Baryon Oscillation Spectroscopic Survey: Cosmological implications from two decades of spectroscopic surveys at the Apache Point Observatory*, *Physical Review D* **103** (2021) 083533 [2007.08991].
- [5] T.M.C. Abbott, M. Aguena, A. Alarcon, S. Allam, O. Alves, A. Amon et al., *Dark Energy Survey Year 3 results: Cosmological constraints from galaxy clustering and weak lensing*, *Physical Review D* **105** (2022) 023520 [2105.13549].
- [6] D. Brout, D. Scolnic, B. Popovic, A.G. Riess, A. Carr, J. Zuntz et al., *The Pantheon+ Analysis: Cosmological Constraints*, *Astrophysical Journal* **938** (2022) 110 [2202.04077].
- [7] H. Miyatake, S. Sugiyama, M. Takada, T. Nishimichi, X. Li, M. Shirasaki et al., *Hyper Suprime-Cam Year 3 results: Cosmology from galaxy clustering and weak lensing with HSC and SDSS using the emulator based halo model*, *Physical Review D* **108** (2023) 123517 [2304.00704].
- [8] S. Sugiyama, H. Miyatake, S. More, X. Li, M. Shirasaki, M. Takada et al., *Hyper Suprime-Cam Year 3 results: Cosmology from galaxy clustering and weak lensing with HSC and SDSS using the minimal bias model*, *Physical Review D* **108** (2023) 123521 [2304.00705].
- [9] DESI Collaboration, A.G. Adame, J. Aguilar, S. Ahlen, S. Alam, D.M. Alexander et al., *DESI 2024 VI: Cosmological Constraints from the Measurements of Baryon Acoustic Oscillations*, *arXiv e-prints* (2024) arXiv:2404.03002 [2404.03002].
- [10] F.J. Qu, B.D. Sherwin, M.S. Madhavacheril, D. Han, K.T. Crowley, I. Abril-Cabezas et al., *The Atacama Cosmology Telescope: A Measurement of the DR6 CMB Lensing Power Spectrum and Its Implications for Structure Growth*, *Astrophysical Journal* **962** (2024) 112 [2304.05202].
- [11] E. Di Valentino, L.A. Anchordoqui, Ö. Akarsu, Y. Ali-Haimoud, L. Amendola, N. Arendse et al., *Cosmology Intertwined III: $f\sigma_8$ and S_8* , *Astroparticle Physics* **131** (2021) 102604 [2008.11285].
- [12] Ž. Ivezić, S.M. Kahn, J.A. Tyson, B. Abel, E. Acosta, R. Allsman et al., *LSST: From Science Drivers to Reference Design and Anticipated Data Products*, *Astrophysical Journal* **873** (2019) 111 [0805.2366].
- [13] D. Spergel, N. Gehrels, C. Baltay, D. Bennett, J. Breckinridge, M. Donahue et al., *Wide-Field Infrared Survey Telescope-Astrophysics Focused Telescope Assets WFIRST-AFTA 2015 Report*, *arXiv e-prints* (2015) arXiv:1503.03757 [1503.03757].
- [14] R. Laureijs, J. Amiaux, S. Arduini, J.L. Auguères, J. Brinchmann, R. Cole et al., *Euclid Definition Study Report*, *arXiv e-prints* (2011) arXiv:1110.3193 [1110.3193].
- [15] E. Krause, T.F. Eifler, J. Zuntz, O. Friedrich, M.A. Troxel, S. Dodelson et al., *Dark Energy Survey Year 1 Results: Multi-Probe Methodology and Simulated Likelihood Analyses*, *arXiv e-prints* (2017) arXiv:1706.09359 [1706.09359].
- [16] X. Li, T. Zhang, S. Sugiyama, R. Dalal, R. Terasawa, M.M. Rau et al., *Hyper Suprime-Cam Year 3 results: Cosmology from cosmic shear two-point correlation functions*, *Physical Review D* **108** (2023) 123518 [2304.00702].
- [17] A.J. Mead, J.A. Peacock, C. Heymans, S. Joudaki and A.F. Heavens, *An accurate halo model*

for fitting non-linear cosmological power spectra and baryonic feedback models, *Monthly Notices of the Royal Astronomical Society* **454** (2015) 1958–1975.

- [18] A. Schneider and R. Teyssier, *A new method to quantify the effects of baryons on the matter power spectrum*, *Journal of Cosmology and Astroparticle Physics* **2015** (2015) 049 [1510.06034].
- [19] G. Aricò, R.E. Angulo, S. Contreras, L. Ondaro-Mallea, M. Pellejero-Ibañez and M. Zennaro, *The BACCO simulation project: a baryonification emulator with neural networks*, *Monthly Notices of the Royal Astronomical Society* **506** (2021) 4070 [2011.15018].
- [20] T. Eifler, E. Krause, S. Dodelson, A.R. Zentner, A.P. Hearin and N.Y. Gnedin, *Accounting for baryonic effects in cosmic shear tomography: determining a minimal set of nuisance parameters using PCA*, *Monthly Notices of the Royal Astronomical Society* **454** (2015) 2451 [1405.7423].
- [21] H.-J. Huang, T. Eifler, R. Mandelbaum and S. Dodelson, *Modelling baryonic physics in future weak lensing surveys*, *Monthly Notices of the Royal Astronomical Society* **488** (2019) 1652 [<https://academic.oup.com/mnras/article-pdf/488/2/1652/28954328/stz1714.pdf>].
- [22] A. Schneider, N. Stoira, A. Refregier, A.J. Weiss, M. Knabenhans, J. Stadel et al., *Baryonic effects for weak lensing. Part I. Power spectrum and covariance matrix*, *Journal of Cosmology and Astroparticle Physics* **2020** (2020) 019 [1910.11357].
- [23] S.G. Stafford, S.T. Brown, I.G. McCarthy, A.S. Font, A. Robertson and R. Poole-McKenzie, *Exploring extensions to the standard cosmological model and the impact of baryons on small scales*, *Monthly Notices of the Royal Astronomical Society* **497** (2020) 3809 [2004.03872].
- [24] M.P. van Daalen, I.G. McCarthy and J. Schaye, *Exploring the effects of galaxy formation on matter clustering through a library of simulation power spectra*, *Monthly Notices of the Royal Astronomical Society* **491** (2020) 2424 [1906.00968].
- [25] A.M. Delgado, D. Anglés-Alcázar, L. Thiele, S. Pandey, K. Lehman, R.S. Somerville et al., *Predicting the impact of feedback on matter clustering with machine learning in CAMELS*, *Monthly Notices of the Royal Astronomical Society* **526** (2023) 5306 [2301.02231].
- [26] W. Elbers, C.S. Frenk, A. Jenkins, B. Li, J.C. Helly, R. Kugel et al., *The FLAMINGO project: the coupling between baryonic feedback and cosmology in light of the S_8 tension*, *arXiv e-prints* (2024) arXiv:2403.12967 [2403.12967].
- [27] G. Parimbelli, M. Viel and E. Sefusatti, *On the degeneracy between baryon feedback and massive neutrinos as probed by matter clustering and weak lensing*, *Journal of Cosmology and Astroparticle Physics* **2019** (2019) 010 [1809.06634].
- [28] N.E. Chisari, A.J. Mead, S. Joudaki, P.G. Ferreira, A. Schneider, J. Mohr et al., *Modelling baryonic feedback for survey cosmology*, *The Open Journal of Astrophysics* **2** (2019) 4 [1905.06082].
- [29] H.-J. Huang, T. Eifler, R. Mandelbaum, G.M. Bernstein, A. Chen, A. Choi et al., *Dark energy survey year 1 results: Constraining baryonic physics in the Universe*, *Monthly Notices of the Royal Astronomical Society* **502** (2021) 6010 [<https://academic.oup.com/mnras/article-pdf/502/4/6010/36524782/stab357.pdf>].
- [30] J. Xu, T. Eifler, V. Miranda, X. Fang, E. Saraivanov, E. Krause et al., *Constraining Baryonic Physics with DES Y1 and Planck data – Combining Galaxy Clustering, Weak Lensing, and CMB Lensing*, *arXiv e-prints* (2023) arXiv:2311.08047 [2311.08047].
- [31] Dark Energy Survey and Kilo-Degree Survey Collaboration, T.M.C. Abbott, M. Aguena, A. Alarcon, O. Alves, A. Amon et al., *DES Y3 + KiDS-1000: Consistent cosmology combining cosmic shear surveys*, *The Open Journal of Astrophysics* **6** (2023) 36 [2305.17173].
- [32] M. Hirschmann, K. Dolag, A. Saro, L. Bachmann, S. Borgani and A. Burkert, *Cosmological*

- simulations of black hole growth: AGN luminosities and downsizing*, *Monthly Notices of the Royal Astronomical Society* **442** (2014) 2304 [1308.0333].
- [33] A.F. Teklu, R.-S. Remus, K. Dolag, A.M. Beck, A. Burkert, A.S. Schmidt et al., *Connecting Angular Momentum and Galactic Dynamics: The Complex Interplay between Spin, Mass, and Morphology*, *Astrophysical Journal* **812** (2015) 29 [1503.03501].
- [34] K. Dolag, E. Komatsu and R. Sunyaev, *SZ effects in the Magneticum Pathfinder simulation: comparison with the Planck, SPT, and ACT results*, *Monthly Notices of the Royal Astronomical Society* **463** (2016) 1797 [<https://academic.oup.com/mnras/article-pdf/463/2/1797/9685287/stw2035.pdf>].
- [35] L.K. Steinborn, K. Dolag, J.M. Comerford, M. Hirschmann, R.-S. Remus and A.F. Teklu, *Origin and properties of dual and offset active galactic nuclei in a cosmological simulation at $z = 2$* , *Monthly Notices of the Royal Astronomical Society* **458** (2016) 1013 [<https://academic.oup.com/mnras/article-pdf/458/1/1013/8181576/stw316.pdf>].
- [36] S. Bocquet, A. Saro, K. Dolag and J.J. Mohr, *Halo mass function: baryon impact, fitting formulae, and implications for cluster cosmology*, *Monthly Notices of the Royal Astronomical Society* **456** (2016) 2361 [1502.07357].
- [37] R.-S. Remus, K. Dolag and T.L. Hoffmann, *The Outer Halos of Very Massive Galaxies: BCGs and their DSC in the Magneticum Simulations*, *Galaxies* **5** (2017) 49 [1709.02393].
- [38] T. Castro, S. Borgani, K. Dolag, V. Marra, M. Quartin, A. Saro et al., *On the impact of baryons on the halo mass function, bias, and cluster cosmology*, *Monthly Notices of the Royal Astronomical Society* **500** (2020) 2316 [<https://academic.oup.com/mnras/article-pdf/500/2/2316/34497990/staa3473.pdf>].
- [39] V. Springel, S.D.M. White, A. Jenkins, C.S. Frenk, N. Yoshida, L. Gao et al., *Simulations of the formation, evolution and clustering of galaxies and quasars*, *Nature* **435** (2005) 629 [astro-ph/0504097].
- [40] V. Springel, T. Di Matteo and L. Hernquist, *Modelling feedback from stars and black holes in galaxy mergers*, *Monthly Notices of the Royal Astronomical Society* **361** (2005) 776 [astro-ph/0411108].
- [41] L. Tornatore, S. Borgani, K. Dolag and F. Matteucci, *Chemical enrichment of galaxy clusters from hydrodynamical simulations*, *Monthly Notices of the Royal Astronomical Society* **382** (2007) 1050 [<https://academic.oup.com/mnras/article-pdf/382/3/1050/18422138/mnras0382-1050.pdf>].
- [42] R.P.C. Wiersma, J. Schaye, T. Theuns, C. Dalla Vecchia and L. Tornatore, *Chemical enrichment in cosmological, smoothed particle hydrodynamics simulations*, *Monthly Notices of the Royal Astronomical Society* **399** (2009) 574 [0902.1535].
- [43] V. Springel and L. Hernquist, *Cosmological smoothed particle hydrodynamics simulations: a hybrid multiphase model for star formation*, *Monthly Notices of the Royal Astronomical Society* **339** (2003) 289 [<https://academic.oup.com/mnras/article-pdf/339/2/289/3230545/339-2-289.pdf>].
- [44] P. Lustig, V. Strazzullo, R.-S. Remus, C. D'Eugenio, E. Daddi, A. Burkert et al., *Massive quiescent galaxies at $z \sim 3$: A comparison of selection, stellar population, and structural properties with simulation predictions*, *Monthly Notices of the Royal Astronomical Society* **518** (2022) 5953 [<https://academic.oup.com/mnras/article-pdf/518/4/5953/47852242/stac3450.pdf>].
- [45] V. Biffi, K. Dolag and A. Merloni, *AGN contamination of galaxy-cluster thermal X-ray emission: predictions for eRosita from cosmological simulations*, *Monthly Notices of the Royal Astronomical Society* **481** (2018) 2213 [<https://academic.oup.com/mnras/article-pdf/481/2/2213/25739502/sty2436.pdf>].

- [46] M. McDonald, B.A. Benson, A. Vikhlinin, K.A. Aird, S.W. Allen, M. Bautz et al., *The Redshift Evolution of the Mean Temperature, Pressure, and Entropy Profiles in 80 SPT-Selected Galaxy Clusters*, *Astrophysical Journal* **794** (2014) 67 [1404.6250].
- [47] N. Gupta, A. Saro, J.J. Mohr, K. Dolag and J. Liu, *SZE observables, pressure profiles and centre offsets in Magneticum simulation galaxy clusters*, *Monthly Notices of the Royal Astronomical Society* **469** (2017) 3069 [https://academic.oup.com/mnras/article-pdf/469/3/3069/17653476/stx715.pdf].
- [48] J. Salcido, I.G. McCarthy, J. Kwan, A. Upadhye and A.S. Font, *SP(k) - a hydrodynamical simulation-based model for the impact of baryon physics on the non-linear matter power spectrum*, *Monthly Notices of the Royal Astronomical Society* **523** (2023) 2247 [2305.09710].
- [49] M. Angelinelli, S. Ettori, K. Dolag, F. Vazza and A. Ragagnin, *Mapping ‘out-of-the-box’ the properties of the baryons in massive halos*, *Astronomy and Astrophysics* **663** (2022) L6 [2206.08382].
- [50] M. Angelinelli, S. Ettori, K. Dolag, F. Vazza and A. Ragagnin, *Redshift evolution of the baryon and gas fraction in simulated groups and clusters of galaxies*, *Astronomy and Astrophysics* **675** (2023) A188 [2305.09733].
- [51] I.G. McCarthy, J. Schaye, S. Bird and A.M.C. Le Brun, *The BAHAMAS project: calibrated hydrodynamical simulations for large-scale structure cosmology*, *Monthly Notices of the Royal Astronomical Society* **465** (2017) 2936 [1603.02702].
- [52] E. Komatsu, K.M. Smith, J. Dunkley, C.L. Bennett, B. Gold, G. Hinshaw et al., *Seven-year Wilkinson Microwave Anisotropy Probe (WMAP) Observations: Cosmological Interpretation*, *Astrophysical Journal Supplement Series* **192** (2011) 18 [1001.4538].
- [53] J. Schaye, R.A. Crain, R.G. Bower, M. Furlong, M. Schaller, T. Theuns et al., *The EAGLE project: simulating the evolution and assembly of galaxies and their environments*, *Monthly Notices of the Royal Astronomical Society* **446** (2015) 521 [1407.7040].
- [54] M. Vogelsberger, S. Genel, V. Springel, P. Torrey, D. Sijacki, D. Xu et al., *Properties of galaxies reproduced by a hydrodynamic simulation*, *Nature* **509** (2014) 177 [1405.1418].
- [55] V. Springel, R. Pakmor, A. Pillepich, R. Weinberger, D. Nelson, L. Hernquist et al., *First results from the IllustrisTNG simulations: matter and galaxy clustering*, *Monthly Notices of the Royal Astronomical Society* **475** (2018) 676 [1707.03397].
- [56] N. Khandai, T. Di Matteo, R. Croft, S. Wilkins, Y. Feng, E. Tucker et al., *The MassiveBlack-II simulation: the evolution of haloes and galaxies to $z \sim 0$* , *Monthly Notices of the Royal Astronomical Society* **450** (2015) 1349 [https://academic.oup.com/mnras/article-pdf/450/2/1349/3020639/stv627.pdf].
- [57] Y. Dubois, C. Pichon, C. Welker, D. Le Borgne, J. Devriendt, C. Laigle et al., *Dancing in the dark: galactic properties trace spin swings along the cosmic web*, *Monthly Notices of the Royal Astronomical Society* **444** (2014) 1453 [1402.1165].
- [58] A.M.C. Le Brun, I.G. McCarthy, J. Schaye and T.J. Ponman, *Towards a realistic population of simulated galaxy groups and clusters*, *Monthly Notices of the Royal Astronomical Society* **441** (2014) 1270 [https://academic.oup.com/mnras/article-pdf/441/2/1270/3656211/stu608.pdf].
- [59] S. Genel, M. Vogelsberger, V. Springel, D. Sijacki, D. Nelson, G. Snyder et al., *Introducing the Illustris project: the evolution of galaxy populations across cosmic time*, *Monthly Notices of the Royal Astronomical Society* **445** (2014) 175 [1405.3749].
- [60] W. Cui, S. Borgani and G. Murante, *The effect of active galactic nuclei feedback on the halo mass function*, *Monthly Notices of the Royal Astronomical Society* **441** (2014) 1769 [1402.1493].

- [61] M. Velliscig, M.P. van Daalen, J. Schaye, I.G. McCarthy, M. Cacciato, A.M.C. Le Brun et al., *The impact of galaxy formation on the total mass, mass profile and abundance of haloes*, *Monthly Notices of the Royal Astronomical Society* **442** (2014) 2641 [1402.4461].
- [62] K.T.E. Chua, M. Vogelsberger, A. Pillepich and L. Hernquist, *The impact of galactic feedback on the shapes of dark matter haloes*, *Monthly Notices of the Royal Astronomical Society* **515** (2022) 2681 [2109.00012].
- [63] J. Kwan, S. Bhattacharya, K. Heitmann and S. Habib, *Cosmic Emulation: The Concentration-Mass Relation for w CDM Universes*, *Astrophysical Journal* **768** (2013) 123 [1210.1576].
- [64] A. Ragagnin, A. Saro, P. Singh and K. Dolag, *Cosmology dependence of halo masses and concentrations in hydrodynamic simulations*, *Monthly Notices of the Royal Astronomical Society* **500** (2021) 5056 [2011.05345].
- [65] D. López-Cano, R.E. Angulo, A.D. Ludlow, M. Zennaro, S. Contreras, J. Chaves-Montero et al., *The cosmology dependence of the concentration-mass-redshift relation*, *Monthly Notices of the Royal Astronomical Society* **517** (2022) 2000 [2207.13718].
- [66] J. Schaye, R. Kugel, M. Schaller, J.C. Helly, J. Braspenning, W. Elbers et al., *The FLAMINGO project: cosmological hydrodynamical simulations for large-scale structure and galaxy cluster surveys*, *Monthly Notices of the Royal Astronomical Society* **526** (2023) 4978 [2306.04024].
- [67] V. Miranda, P. Rogozenski and E. Krause, *Interpreting internal consistency of DES measurements*, *Monthly Notices of the Royal Astronomical Society* **509** (2022) 5218 [2009.14241].
- [68] E. Krause and T. Eifler, *cosmolike - cosmological likelihood analyses for photometric galaxy surveys*, *Monthly Notices of the Royal Astronomical Society* **470** (2017) 2100 [1601.05779].
- [69] J. Torrado and A. Lewis, *Cobaya: code for Bayesian analysis of hierarchical physical models*, *Journal of Cosmology and Astroparticle Physics* **2021** (2021) 057 [2005.05290].
- [70] A. Lewis and A. Challinor, “CAMB: Code for Anisotropies in the Microwave Background.” Astrophysics Source Code Library, record ascl:1102.026, Feb., 2011.
- [71] X. Fang, E. Krause, T. Eifler and N. MacCrann, *Beyond limber: efficient computation of angular power spectra for galaxy clustering and weak lensing*, *Journal of Cosmology and Astroparticle Physics* **2020** (2020) 010.
- [72] S. Bridle and L. King, *Dark energy constraints from cosmic shear power spectra: impact of intrinsic alignments on photometric redshift requirements*, *New Journal of Physics* **9** (2007) 444 [0705.0166].
- [73] R. Takahashi, M. Sato, T. Nishimichi, A. Taruya and M. Oguri, *Revising the halofit model for the nonlinear matter power spectrum*, *The Astrophysical Journal* **761** (2012) 152.
- [74] The LSST Dark Energy Science Collaboration, R. Mandelbaum, T. Eifler, R. Hložek, T. Collett, E. Gawiser et al., *The LSST Dark Energy Science Collaboration (DESC) Science Requirements Document*, *arXiv e-prints* (2018) arXiv:1809.01669 [1809.01669].
- [75] D. Foreman-Mackey, D.W. Hogg, D. Lang and J. Goodman, *emcee: The MCMC Hammer*, *Publications of the Astronomical Society of the Pacific* **125** (2013) 306 [1202.3665].
- [76] X. Fang, T. Eifler and E. Krause, *2D-FFTLg: efficient computation of real-space covariance matrices for galaxy clustering and weak lensing*, *Monthly Notices of the Royal Astronomical Society* **497** (2020) 2699 [https://academic.oup.com/mnras/article-pdf/497/3/2699/33638835/staa1726.pdf].
- [77] S.S. Boruah, T. Eifler, V. Miranda and P.M.S. Krishanth, *Accelerating cosmological inference with Gaussian processes and neural networks - an application to LSST Y1 weak lensing and*

galaxy clustering, *Monthly Notices of the Royal Astronomical Society* **518** (2023) 4818 [[2203.06124](#)].

- [78] M. Haider, D. Steinhauser, M. Vogelsberger, S. Genel, V. Springel, P. Torrey et al., *Large-scale mass distribution in the Illustris simulation*, *Monthly Notices of the Royal Astronomical Society* **457** (2016) 3024 [[1508.01525](#)].
- [79] A.M.C. Le Brun, I.G. McCarthy, J. Schaye and T.J. Ponman, *Towards a realistic population of simulated galaxy groups and clusters*, *Monthly Notices of the Royal Astronomical Society* **441** (2014) 1270 [[1312.5462](#)].
- [80] X. Fang, E. Krause, T. Eifler, S. Ferraro, K. Benabed, R.S. Pranjali et al., *Cosmology from weak lensing, galaxy clustering, CMB lensing, and tSZ - I. $10 \times 2pt$ modelling methodology*, *Monthly Notices of the Royal Astronomical Society* **527** (2024) 9581 [[2308.01856](#)].